

## Distant clock synchronization using entangled photon pairs

Alejandra Valencia,<sup>a)</sup> Giuliano Scarcelli, and Yanhua Shih

*Department of Physics, University of Maryland, Baltimore County, Baltimore, Maryland 21250*

(Received 27 May 2004; accepted 2 August 2004)

We report a proof-of-principle experiment on distant clock synchronization. Besides the achievement of picosecond resolution at 3 km distance, this experiment demonstrated a concept for high-accuracy nonlocal timing and positioning based on the quantum feature of entangled states.

© 2004 American Institute of Physics. [DOI: 10.1063/1.1797561]

Accurate timing and positioning metrological measurements are important for both fundamental research and practical applications. In particular, distant clock synchronization has attracted a great deal of attention in recent years due to its essential role in the Global Positioning System and telecommunications.<sup>1</sup>

Modern clocks have been improved to such a level,<sup>2</sup> that the resolution and accuracy of the comparison techniques have become the limiting factors to determine their relative rates and synchronization. There are two standard methods for synchronizing two distant clocks: the classic Einstein protocol<sup>3</sup> and the Eddington slow transportation method.<sup>4</sup> Both methods have certain limitations and difficulties in high accuracy nonlocal synchronization in which relativistic effects, such as the rotating disk problem, have to be taken into consideration. Einstein protocol is a two-way method, hence, it requires (i) an accurate knowledge of the one-way speed of light, which has not been measured conclusively on rotating reference systems and (ii) the light propagation path to be the same in each direction. The Eddington transportation method relies on the physical movement of a clock, therefore, this method is not practical for space applications. Recently, the nonlocal characteristics of entangled states have brought attention to possible protocols of high resolution clock synchronization.<sup>5–7</sup>

In this letter we wish to report an experimental proof-of-principle demonstration of a concept, based on the nonlocal feature of entangled states, that can be practically implemented for certain metrology applications such as high-accuracy one-way synchronization of clocks and high-accuracy positioning.

Our method relies on the measurement of the second-order correlation function of entangled states. In particular, we consider the entangled photon pairs produced in a cw pumped spontaneous parametric down conversion (SPDC).<sup>8</sup> Very roughly speaking, the process of SPDC involves sending a pump laser beam into a nonlinear material, such as a noncentrosymmetric crystal. Occasionally, the nonlinear interaction inside the crystal leads to the annihilation of a high frequency pump photon and the creation of two lower frequency photons named as signal and idler. The creation time of either signal photon or idler photon is unknown; however, if the signal photon is registered at a certain time, the detection time of the idler photon can only happen at a unique precise time. In the reported experiment, both the signal photon and the idler photon are in the form of continuous wave,

i.e.,  $\Delta t = \infty$ , nevertheless the time correlation measurement of the signal–idler at a distance of 3 km has shown uncertainty in the order of a picosecond.

According to quantum field theory, the probability of having a joint photodetection event at space–time points  $(\mathbf{r}_1, t_1)$  and  $(\mathbf{r}_2, t_2)$  is proportional to the second-order correlation function of the fields<sup>9</sup>

$$G^{(2)}(\mathbf{r}_1, t_1; \mathbf{r}_2, t_2) = \langle E^{(-)}(\mathbf{r}_1, t_1) E^{(-)}(\mathbf{r}_2, t_2) E^{(+)}(\mathbf{r}_2, t_2) \times E^{(+)}(\mathbf{r}_1, t_1) \rangle, \quad (1)$$

where  $E^{(-)}$  and  $E^{(+)}$  are the negative-frequency and the positive-frequency field operators of the detection events at space–time points  $(\mathbf{r}_1, t_1)$  and  $(\mathbf{r}_2, t_2)$ . For the two-photon entangled state of SPDC,  $G^{(2)}(\mathbf{r}_1, t_1; \mathbf{r}_2, t_2)$  can be written as the modulus square of a two-photon effective wave function, or biphoton:

$$G^{(2)}(\mathbf{r}_1, t_1; \mathbf{r}_2, t_2) = |\langle 0 | E^{(+)}(\mathbf{r}_2, t_2) E^{(+)}(\mathbf{r}_1, t_1) | \Psi \rangle|^2 \equiv |\psi(\mathbf{r}_1, t_1; \mathbf{r}_2, t_2)|^2, \quad (2)$$

where  $|0\rangle$  stands for the vacuum and  $|\Psi\rangle$  is the state of the signal–idler photon pair.<sup>10</sup>

The two-photon effective wave function is calculated to be

$$\Psi(r_1, t_1; r_2, t_2) = e^{-i(\omega_s^0 \tau_1 + \omega_i^0 \tau_2)} \mathcal{F}_{\tau_1 - \tau_2} \{f(\Omega)\}, \quad (3)$$

where  $\mathcal{F}_{\tau_1 - \tau_2} \{f(\Omega)\}$  is the Fourier transform of the spectrum amplitude function  $f(\Omega)$ ,  $\tau_j = t_j - r_j/u_j$ ,  $j=1, 2$ , and  $u_j$  is the group velocity at frequencies  $\omega_s^0$  and  $\omega_i^0$  along the optical paths 1 and 2, respectively.  $\omega_s^0$  and  $\omega_i^0$  are the central frequencies of the signal–idler radiation field.

The  $G^{(2)}(r_1, t_1; r_2, t_2)$  function for the two-photon entangled state of SPDC is thus

$$G^{(2)}(r_1, t_1; r_2, t_2) = |\mathcal{F}_{\tau_1 - \tau_2} \{f(\Omega)\}|^2. \quad (4)$$

This function, depending on  $\tau_1 - \tau_2$  is independent of the chosen reference coordinates: it is a Lorentzian invariant.<sup>11</sup> The spectrum amplitude function of the SPDC,  $f(\Omega)$ , provides all the information about the spectrum and the correlation properties of the signal–idler pair and it has been well studied.<sup>8,12</sup>

In the collinear case for type-II and nondegenerate type-I SPDC, the spectral function is calculated as  $f(\Omega) \sim \text{sinc}(DL\Omega/2)$ , where  $L$  is the length of the crystal and  $D = 1/u_s - 1/u_i$  is the inverse group velocity difference for the signal and idler. For an 8 mm LBO crystal pumped at 458 nm (type-II), the estimated width of  $G^{(2)}(t_1 - t_2)$  is about 800 fs. For collinear degenerate type-I SPDC, the spectral

<sup>a)</sup>Electronic mail: avalen1@umbc.edu

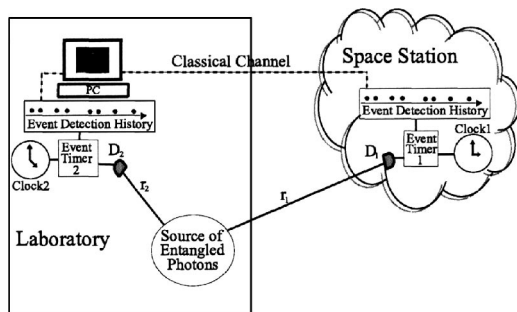


FIG. 1. Schematic setup of a protocol for one-way distant clock synchronization.

function is  $f(\Omega) \sim \text{sinc}(D''L\Omega/2)$  where  $D''$  is the second derivative of the dispersion function of the nonlinear material. In this case, the width of  $G^{(2)}(t_1 - t_2)$  is about 30 fs for the same size LBO crystal. Typical values for the natural width of  $G^{(2)}$  for SPDC are, then, on the order of a few femtoseconds to hundreds of femtoseconds. If  $r_1$  and  $r_2$  are well controlled, the measurement of  $t_1 - t_2$  can reach, in principle, the same order of resolution, making SPDC particularly suitable for implementing protocols for timing and positioning measurements with ultrahigh accuracy.

For example, consider a new protocol for one-way synchronization of two distant clocks: we have clock-1 in a space station and clock-2 in the laboratory (Fig. 1). The signal and idler photons are sent to two photon counting detectors  $D_1$  (in space) and  $D_2$  (on the ground). The photon registration times of the detectors,  $t_1$  and  $t_2$ , are recorded by two “event timers” whose time bases are provided by clock-1 and clock-2, respectively.<sup>13</sup> The individual time history records can be brought together through a classical communication channel for comparison. If the two clocks are synchronized, the joint detection of the signal–idler pair obtained by matching the photon registration time records will show maximum “coincidences.” If the clocks lose their synchronization, one has to rematch the records to achieve maximum coincidences by shifting one of them by a certain amount, that corresponds to how much the two clocks have lost their synchronization. The clocks can be adjusted and kept synchronized accordingly.

The initial synchronization of the two clocks is made in the following way: first we send the signal (with wavelength  $\lambda_s$ ) to detector  $D_1$  and the idler (with wavelength  $\lambda_i$ ) to detector  $D_2$ . The registration time difference,  $t_1 - t_2$ , at  $D_1$  and  $D_2$  is estimated:

$$t_1 - t_2 = \frac{r_1}{u_s} + t_0 - \frac{r_2}{u_i}, \quad (5)$$

where  $t_0$  is the time offset of the two nonsynchronized clocks. Then, we switch the signal and the idler, sending the idler to  $D_1$  and the signal to  $D_2$ . The registration time difference,  $t'_1 - t'_2$  of  $D_1$  and  $D_2$  will now be

$$t'_1 - t'_2 = \frac{r_1}{u_i} + t_0 - \frac{r_2}{u_s}. \quad (6)$$

Subtracting the two registration time differences, we have

$$\Delta t_- = (t_1 - t_2) - (t'_1 - t'_2) = D(r_1 + r_2), \quad (7)$$

where  $D = 1/u_s - 1/u_i$ .  $\Delta t_-$  is obtained from direct measurements and we assumed that  $r_2$  is known ( $D_2$  is in the labo-

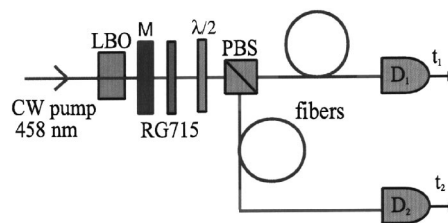


FIG. 2. Schematic setup of the proof-of-principle experiment.

rary). In some cases  $D$  is known or independently measurable, therefore the distance between the space station and the laboratory,  $r_1$ , is predictable through the measurements of  $\Delta t_-$ . In other cases,  $r_1$  may be given or independently measurable, so, the value of  $D$  can be calibrated in the above procedure with ultrahigh accuracy. In both cases substituting into either Eq. (5) or Eq. (6), the time offset  $t_0$  is thus estimated with the same order of accuracy as the measurement of  $t_1 - t_2$  and the clocks are synchronized accordingly. Notice that the measurement can be easily repeated for different values of  $r_2$ , so, for example, even in the case in which both  $D$  and  $r_1$  are unknown, measurements of  $\Delta t_-$  with different known values of  $r_2$  allow the evaluation of  $D$  and  $r_1$  simultaneously.

We performed the proof-of-principle experimental demonstration in the case in which  $r_1$  and  $r_2$  were known: in the laboratory, long optical fibers of known lengths were used to simulate the nonlocal condition. The setup is shown in Fig. 2. A single frequency  $\text{Ar}^+$  laser line of 457.9 nm was used to pump an 8 mm LBO crystal for type-II SPDC. The signal–idler radiations (centered at  $\sim 901$  nm and at  $\sim 931$  nm, respectively) were separated from the pump laser beam by using filtering devices. The orthogonally polarized signal–idler pair was split by means of a polarizing beam splitter. Before the beam splitter, a half-wave plate was placed in order to perform the two measurements described previously: when the wave plate is at  $0^\circ$ , the signal is transmitted to  $D_1$  and the idler reflected to  $D_2$ ; when the wave plate is at  $45^\circ$ , the idler is transmitted to  $D_1$  and the signal is reflected to  $D_2$ . In both measurements, the signal and idler radiation were fed into two 1.5 km-long commercial optical fibers optimized for single-mode operation at 1300 nm. The signal–idler pair was then detected by two single-photon counting detectors. After a large number of signal–idler pair measurements, a histogram of the number of counts against  $t_1 - t_2$  (the resolution of the fast-timing electronics is 3 ps) can be obtained. This distribution function corresponds to the  $G^{(2)}(t_1 - t_2)$  function previously described.<sup>14</sup>

Figure 3 shows the experimental results. The distribution function on the left corresponds to the case of signal- $D_1$  and idler- $D_2$  (half-wave plate at  $0^\circ$ ) while the distribution function on the right corresponds to the case of idler- $D_1$  and signal- $D_2$  (half-wave plate at  $45^\circ$ ). The presence of multiple peaks on each individual distribution function is a consequence of intermodal dispersion in optical fibers, which is a known effect in fiber optics.<sup>15</sup>

The calculated width of the effective two-photon wave function from an 8 mm type-II LBO SPDC, without the long optical fibers, is about 800 fs. The measured width of  $G^{(2)}(t_1 - t_2)$ , with the fibers, is around 750 ps. There are two contributions for the broadening of the  $G^{(2)}$  function: (i) dispersion in the optical fiber, which may be compensated

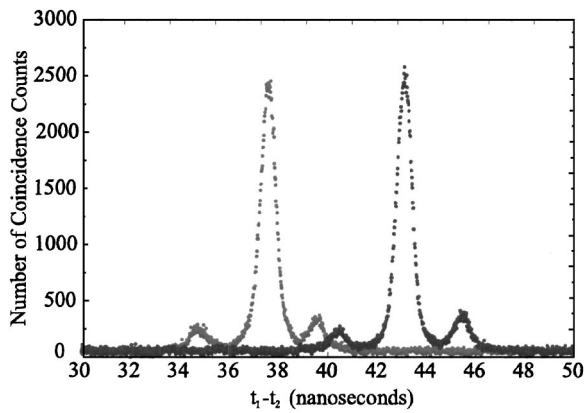


FIG. 3. A typical histogram, the number of counts vs detection time difference  $t_1-t_2$ . Curve on the left: half-wave plate at  $0^\circ$ , Curve on the right: half-wave plate at  $45^\circ$ . The presence of side-peaks is due to the excitation of side-modes in the fiber.

nonlocally<sup>12,16</sup> (the compensation is not included in this proof-of-principle experiment); (ii) the time jitter of the photodetector. The behavior of the biphoton in dispersive medium has been previously studied.<sup>12</sup> Using two fibers of 1.5 km length, the far-field zone condition is satisfied. Therefore, we expect  $G^{(2)}(t_1-t_2)$  to take the shape of the spectrum function of the type-II SPDC  $|f(\Omega)|^2$  with a full width at half maximum of 600 ps. Figure 4 shows the central peak of the experimental data (for the case of half-wave plate at  $45^\circ$ ) compared with the theoretical expectation when the broadening contributions of (i) and (ii) are taken into consideration. The fitting parameters  $k_s''$  and  $k_i''$  of the signal-idler radiations,  $2.76 \times 10^{-28}$  and  $2.96 \times 10^{-28}$  s<sup>2</sup>/cm, respectively, are

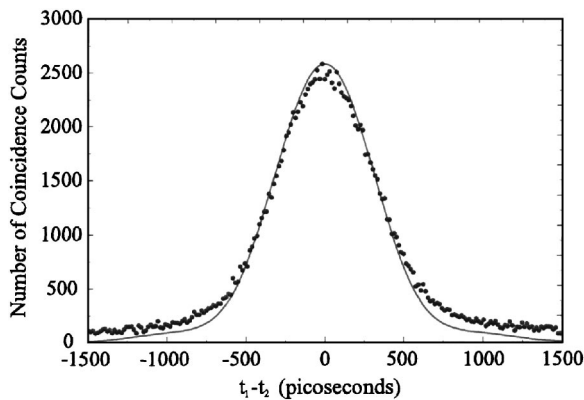


FIG. 4. Central peak of the measured distribution function of  $t_1-t_2$ . The solid line is a theoretical fitting curve of  $G^{(2)}$  considering the broadening contributions of the propagation dispersion and the jitter of the photon counting detectors.

in agreement with the values specified by the manufacturer of the optical fiber.

By measuring the displacement of the central peak when the half-wave plate is rotated from  $0^\circ$  to  $45^\circ$  ( $\Delta t = 5432 \pm 1$  ps), and knowing the length of the fibers, the experimental value for  $D$ , using Eq. (7), was found to be  $1799.9 \pm 0.4$  ps/km, in agreement with the parameters of the fibers. Substituting the estimated value of  $D$  into either Eq. (5) or Eq. (6), the time offset is measured to be  $t_0 = 40369 \pm 1$  ps, which has the same order of accuracy of the  $t_1-t_2$  measurement.

In conclusion, we performed a high accuracy (picosecond) proof-of-principle experiment on distant clock synchronization (3 km). Besides the implementation of the one-way clock synchronization protocol, this experiment has also demonstrated a concept of quantum metrology for high accuracy nonlocal timing and positioning.

The authors thank M. H. Rubin, M. D'Angelo, and D. Hudson for helpful discussions; G. Carter and H. Jiao for the loan of the fibers. This work was supported, in part, by NASA-CASPR program, NSF, and ONR.

<sup>1</sup>T. B. Bahder, gr-qc/0405001.

<sup>2</sup>W. Wayt Gibbs, Sci. Am., special issue (September 2002).

<sup>3</sup>A. Einstein, Ann. Phys. (Leipzig) **17**, 891 (1905).

<sup>4</sup>A. S. Eddington, *The Mathematical Theory of Relativity* (Chelsea, New York, 1924).

<sup>5</sup>R. Josza, D. S. Abrams, J. P. Dowling, and C. P. Williams, Phys. Rev. Lett. **85**, 2010 (2000).

<sup>6</sup>V. Giovannetti, S. Lloyd, and L. Maccone, Nature (London) **412**, 417 (2001).

<sup>7</sup>V. Giovannetti, S. Lloyd, L. Maccone, and F. N. C. Wong, Phys. Rev. Lett. **87**, 117902 (2001).

<sup>8</sup>D. N. Klyshko, *Photons and Nonlinear Optics* (Gordon & Breach, New York, 1988).

<sup>9</sup>R. J. Glauber, Phys. Rev. **130**, 2529 (1963); **131**, 2766 (1963).

<sup>10</sup>M. H. Rubin, D. N. Klyshko, Y. H. Shih, and A. V. Sergienko, Phys. Rev. A **50**, 5122 (1994).

<sup>11</sup>T. B. Bahder, Phys. Rev. D **68**, 063005 (2003).

<sup>12</sup>A. Valencia, M. V. Chekhova, A. Trifonov, and Y. Shih, Phys. Rev. Lett. **88**, 183601 (2002).

<sup>13</sup>C. Steggerda, C. B. Clarke, J. M. Heinick, D. McClure, M. Selden, R. Stringfellow, and G. Bianco, in *Proceedings of the 10th International Workshop on Laser Ranging Instrumentation, Shanghai, China* (Chinese Academy of Sciences Press, Beijing, China, 1996).

<sup>14</sup>L. Mandel and E. Wolf, *Optical Coherence and Quantum Optics* (Cambridge University Press, Cambridge, 1995).

<sup>15</sup>The fibers are optimized for single mode operation at 1300 nm. For the operating wavelengths (approximately 901 and 931 nm) two modes are excited (Ref. 17). These modes have different group velocities that result in different time delays and cause the side peaks.

<sup>16</sup>J. D. Franson, Phys. Rev. A **45**, 3126 (1992).

<sup>17</sup>J. M. Senior, *Optical Fiber Communications Principles and Practice* (Prentice-Hall International, Cambridge, 1992).